

Diode Power Probe Measurements of Wireless Signals

Hugo Gomes^{1,2}, Alejandro R. Testera³, Nuno Borges Carvalho¹,
Mónica F. Barciela³, Kate A. Remley⁴

1 – Instituto de Telecomunicações – Universidade de Aveiro – Portugal

2 – Instituto Politécnico de Leiria – Portugal, 3 - Universidad de Vigo, Spain

4 – NIST Electromagnetics Division, Boulder, CO, USA, 80305

Abstract— A new view of diode power probes is presented in this paper. It is shown analytically, by simulations, and with measurements, that calibration procedures for diode power probes should be rethought when measuring new wireless standard types of signals. In this respect, an improved analysis of long term-memory effects and the behavior of power probes when in the presence of wideband and high peak-to-average-power ratio signals is analyzed and studied. We show that a power probe calibrated with a single-tone sinusoidal excitation can provide erroneous values when used with modulated signals. This is ascribed to the low-frequency response imposed by the power probe baseband circuit. This hypothesis is first theoretically demonstrated by use of a Volterra series and then validated by simulations and measurements using a diode power probe. A similar approach is used for high PAPR signals when using multisines as the excitation signal.

Index Terms—Diode Power Probe, Long-term Memory Effects, Nonlinear Devices, Power Measurement, PAPR.

I. INTRODUCTION

POWER probes based on diodes have been used for many years for high-speed power measurements, and the results have been quite satisfactory when the power being measured is the power of a simple signal such as a sinusoid [1-3]. The nonlinearity of the diode in these probes rectifies an RF signal, providing a representation of the RF power through the output DC voltage.

However, the nonlinear response of the power probe may be non constant over the bandwidth of the RF input signal and may impact the time domain evolution of the signal. This can be an issue when measuring signals for state-of-the-art wireless systems that have wide bandwidths and high values of peak-to-average power ratio (PAPR).

The bandwidth-dependent behavior of the power probe can be ascribed to the dynamic interaction of its baseband impedance response and the low-frequency voltage and current excited by the nonlinear device under test under modulated-signal excitation [4]. If not corrected, these dynamic effects may impact the reliability of the measurements. Commercially available microwave power sensors have been designed to work in a 50 Ω environment, eliminating impedance mismatches. However, simple diode power detector circuits are used in, for example, cell phone applications, to monitor the received power from the base station. For these circuits, the baseband embedding impedance can play a key role.

Moreover, the high value of PAPR and switched performance of modern wireless signals may also interact with the nonlinear characteristic of the diode probe. Use of high PAPR signals may also yield erroneous power results, as was seen in [5] for code-division-multiple-access (CDMA) Intermediate Standard 1995 (IS-95) signals.

In this paper, we will study and analyze the impact of dynamic long-term memory effects on measurements made with diode power probes. We will study their behavior in the presence of high PAPR signals and provide methods for user

characterization of diode power probes. This analysis will be conducted by comparing single-tone, two-tone and multisine excitations of a representative power probe. The DC voltage corresponding to the detected power will be studied to explain the changes caused by dynamic effects.

Long-term memory effects in power amplifiers have been studied for many years. They are normally attributed to the low-frequency behavior of a transistor or amplifier, often due to the bias networks. Both input and output bias matching networks may cause these effects [6]. The frequency response of these external networks imposes a change in the nonlinear behavior of the device, mainly introducing asymmetries in the upper and lower third-order intermodulation distortion products as a function of the excitation bandwidth.

In envelope detectors, this low-frequency interaction is also intuitively expected. This is because, for this case, the objective is to down-convert the signal from RF to the baseband.

The nonlinear distortion created by diode power probes is not so obvious. Because we are searching for the DC voltage created by the rectification of the diode, we may not expect that the effects of nonlinear distortion in the kilohertz or megahertz range would affect this DC value [1-3]. However, the nonlinearity of the junction capacitance of the diode means that the superposition theorem is not valid anymore. As a result, the output of the diode is different for single or multiple tones. While the use of a single sinusoid does not create any baseband spurious signals, in a multisine arrangement, the baseband generated signals have a bandwidth equivalent to the RF one.

At the same time, new wireless standards are also imposing severe changes in the time-domain envelope, mainly evaluated using their PAPR, which can severely limit the range of operation of diode power sensors [7]. Unfortunately typical calibration procedures are used for constant-envelope signals, such as single sinusoids, which do not create the fast variations of modern wireless signals.

In [8], the authors conducted a preliminary study of the effects of baseband impedance terminations on the accuracy of the DC voltage measured by the probe. In [9], a simple study of the differences between one tone measurements and modulated signals was carried out.

In the present work, we will further study the impact of these terminations, first for a single sinusoid and then for a multisine signal, including high PAPR signals having various statistical characteristics. We also will develop and improve methods to predict the effect of the baseband impedance on the measured DC values.

Actually the explanation of different behaviors of the probe when in presence of signals with quite different PAPR values

relationship, due to the fact that the $Y_{dc}(0)$ is always a group of complex conjugated mixing products, as can be seen by the fact that A_1 and A_2 always appear squared. Nevertheless, from expression (9) we see that the baseband impedance may also affect the DC value.

In order to better understand how the baseband impedance affects the DC value, consider that the output matching network presents a low-pass behavior. This means that $Z(\omega) \approx 0$ for RF frequencies, but is different from zero at very low frequencies. In this case, H_2 and H_4 simplify to

$$H_2(\omega_1, \omega_2) = \frac{Z(\omega_1 + \omega_2) \cdot k_2}{1 + k_1 Z(\omega_1 + \omega_2)} \quad (10)$$

$$H_4(\omega_1, \omega_2, \omega_3, \omega_4) = \frac{Z(\omega_1 + \omega_2 + \omega_3 + \omega_4) \times \left[k_2 \left(\frac{1}{3} H_2[\omega_1, \omega_2] \cdot H_2[\omega_3, \omega_4] + \frac{1}{3} H_2[\omega_1, \omega_4] \cdot H_2[\omega_2, \omega_3] + \dots \right) + k_3 \left(-\frac{1}{2} H_2[\omega_1, \omega_2] - \frac{1}{2} H_2[\omega_1, \omega_4] - \frac{1}{2} H_2[\omega_2, \omega_4] - \frac{1}{2} H_2[\omega_3, \omega_4] + \dots \right) + k_4 \right]}{1 + k_1 Z(\omega_1 + \omega_2 + \omega_3 + \omega_4)} \quad (11)$$

If expressions (9) to (11) are closely studied, we see that, for a two-tone case, the term $H_4(\omega_1; -\omega_1; \omega_2; -\omega_2)$ will be

$$H_4(\omega_1, -\omega_1, \omega_2, -\omega_2) = \frac{Z(\omega_1 - \omega_1 + \omega_2 - \omega_2) \times \left[k_2 \left(\frac{1}{3} H_2[\omega_1, -\omega_1] \cdot H_2[\omega_2, -\omega_2] + \frac{1}{3} H_2[\omega_1, -\omega_2] \cdot H_2[-\omega_1, \omega_2] + \dots \right) + k_3 \left(-\frac{1}{2} H_2[\omega_1, -\omega_1] - \frac{1}{2} H_2[\omega_2, -\omega_2] - \frac{1}{2} H_2[\omega_1, -\omega_2] - \frac{1}{2} H_2[-\omega_1, \omega_2] + \dots \right) + k_4 \right]}{1 + k_1 Z(\omega_1 - \omega_1 + \omega_2 - \omega_2)} \quad (12)$$

Looking further, for instance, at $H_2(\omega_1, -\omega_2)$, it can be seen that

$$H_2(\omega_1, -\omega_2) = \frac{Z(\omega_1 - \omega_2) \cdot k_2}{1 + k_1 Z(\omega_1 - \omega_2)} \quad (13)$$

This clearly illustrates that the DC value depends on the impedance that appears at $\omega_1 - \omega_2$.

To illustrate the concept behind these formulas, an output matching circuit presenting a load impedance having the response shown in Fig. 2 will be used. This impedance was designed to exhibit a resonance around 750 kHz, to simulate the memory effect pattern. We use this impedance in (4) to (7), together with standard diode model values [6]. In this case, $Y_{dc}(0)$ will have different values for different excitations, as expected.

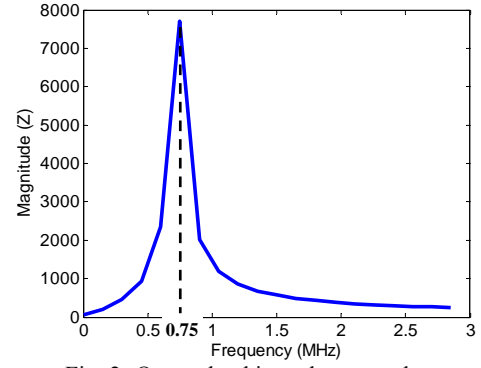


Fig. 2- Output load impedance used as an illustrative example.

The DC response for single-tone and two-tone excitations is shown in Fig. 3. In the one-tone case, we sweep the frequency of the tone over a 2.5 MHz frequency range near the carrier. In the two-tone case, we sweep the tone spacing from near 0 Hz to 2.5 MHz.

As shown Fig. 3, with a single tone, the DC output voltage is equal for all values of frequency. With two excitation tones, the resonance in the baseband impedance has a noticeable effect on the DC output. For the case shown here, the maximum deviation appears at the resonant frequency.

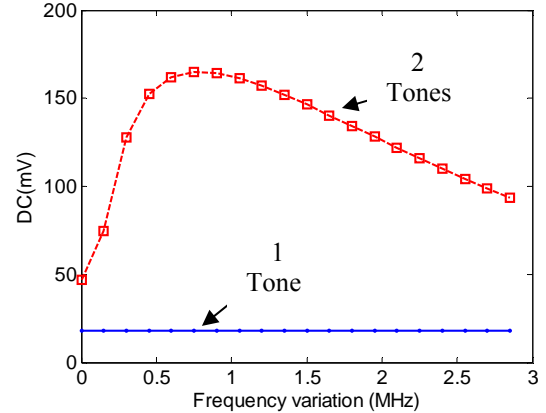


Fig. 3- Output voltage of the diode probe obtained through the Volterra model.

This mathematical approach illustrates that the calibration of the overall system with a single sinusoid will not guarantee the calibration of the diode power probe for other types of excitations because they may be corrupted by long-term memory effects.

III. BANDWIDTH-DEPENDENT PROBE BEHAVIOR

In order to validate the mathematical concepts presented in the previous section, a diode power detector circuit designed for operation at 5.8 GHz, was simulated by use of a commercially available circuit simulator. The schematic of the simulated circuit is presented in Fig. 4. The bias circuit will be used as a way to guarantee that the circuit will work in its valid operating range, although the bias can be set to zero when desired.

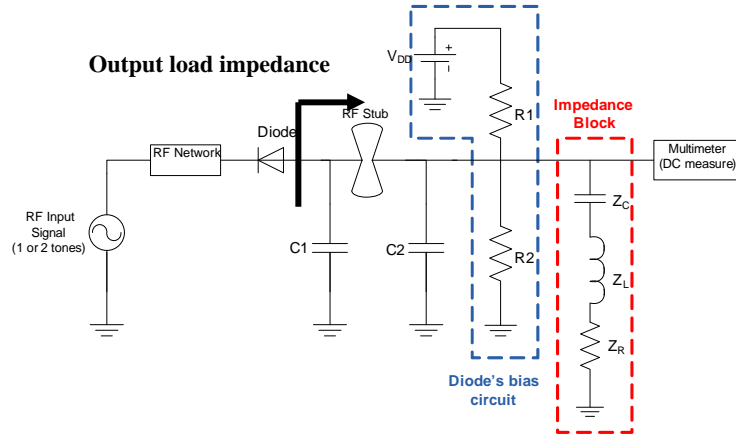


Fig. 4 – Schematic of the diode power detector circuit used in our simulations.

For modeling the Schottky diode behavior, the Vigo measurement-based model was used [10]. This model is a time-domain, table-based nonlinear model, extracted from DC and small signal measurements. As can be seen in Fig. 5, the model consists of a linear extrinsic network and a nonlinear intrinsic one. The extrinsic network models the device parasitics and the influence of the packaging. The intrinsic part is composed of nonlinear current and charge sources that are table-based and bias dependent. The diode nonlinear current function is directly extracted from measured diode DC-IV data. The nonlinear charge function is obtained from single-frequency, small-signal S-parameter measurements versus bias by using an integration procedure based on smoothing B-splines. Both intrinsic nonlinear functions are defined as a function of the intrinsic voltage and they are spline interpolated during the simulation.

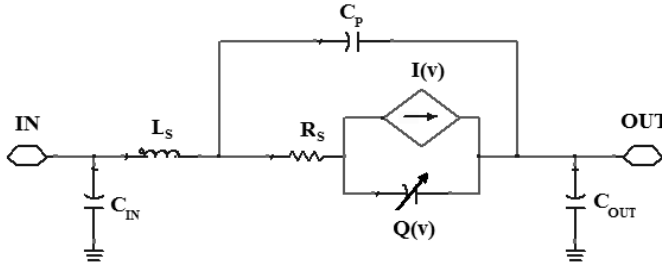


Fig. 5 - Diode nonlinear model topology.

An analytic soft reverse-breakdown approach is added to the current function formulation to model the behavior of the diode under high-input RF power drive, given by

$$(14)$$

This is necessary to improve the model extrapolation at high power levels, showing the expected saturated DC response when used in the detector circuit. As described, the approach presented here is an improvement of the one used in [10]. Figs. 6 and 7 show the model's behavior under DC, single-tone and two-tone operating conditions. The measured results shown here are based on the assumptions that the test equipment is operating within manufacturers' specifications ($\pm 0.7\%$ for

the DC voltmeter, and ± 0.5 dB for the VNA), and that the sources of random error are negligible.

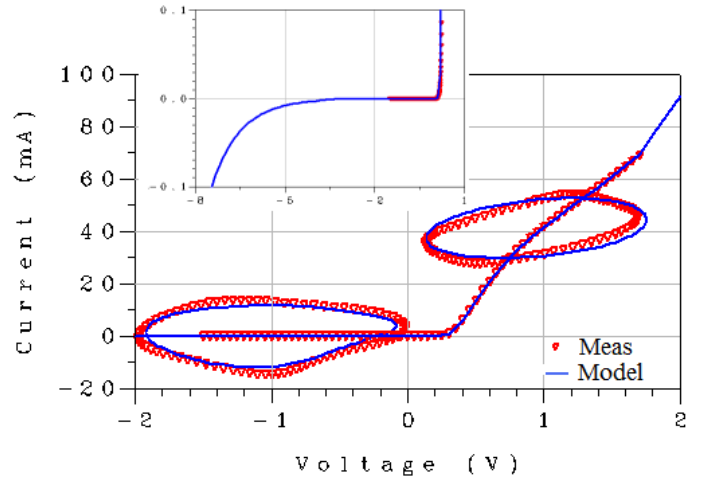


Fig. 6 - Measured and modeled DC (including the soft reverse breakdown simulations) and time domain RF waveforms at two bias points: $f_0=5.8$ GHz, $P_{in}=7$ dBm. Bias point 1: $V=-1$ V ($I=-33$ nA). Bias point 2: $V=1$ V ($I=35.8$ mA).

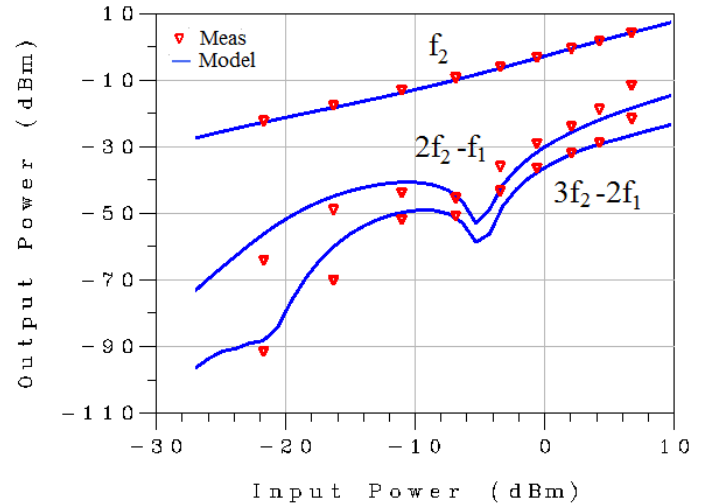


Fig. 7 – Measured and modeled diode two-tone large-signal behavior. $f_1=5.8$ GHz-0.05 MHz, $f_2=5.8$ GHz+0.05 MHz, Bias point: $V=0.1375$ V ($I=3\mu$ A).

An output-matching circuit was built in order to optimize the performance of the circuit, both at 5.8 GHz and at baseband, presenting a low-pass filter behavior. An output load impedance with a resonance at 2.25 MHz was inserted in order to clearly mimic the effect of the baseband impedance, as illustrated in Fig. 8.

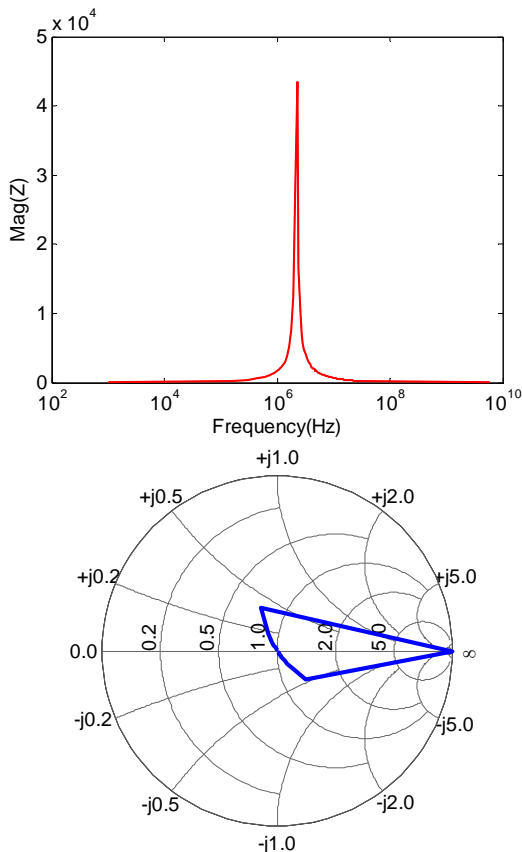
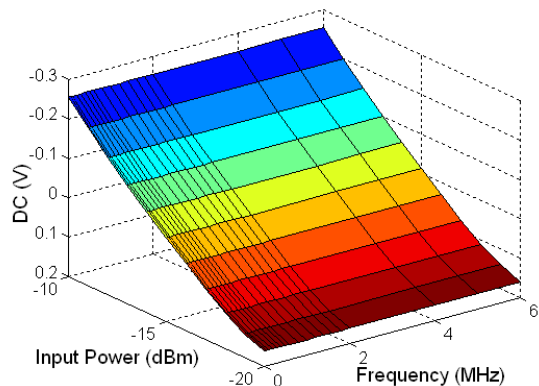


Fig. 8 – Diode’s simulated output load impedance.

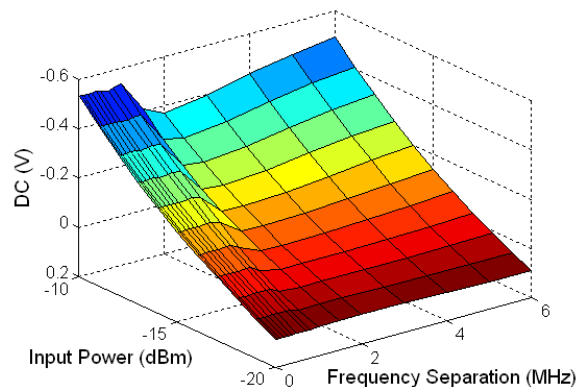
To capture the behavior of the diode power detector, two simulations were conducted. In the first, a one-tone excitation was centered at 5.8 GHz and swept in frequency within a 6 MHz band around the carrier. The results are shown in Fig. 9(a). In the second simulation, a two-tone excitation was centered at 5.8 GHz. In this case, the tone separation was swept from 0 to 6 MHz. The power of each tone was varied from -20 dBm to -10 dBm. Results are shown in Fig. 9(b).

We expect that the voltage measured at the output of the diode probe for the two-tone excitation would be almost twice that of the voltage measured with the single tone, presenting the same power. In fact, this is the case for frequency separation near 0 Hz.

But for other frequency spacing values, especially close to the resonance frequency, the detector’s output for the two-tone excitation changes significantly. The one-tone simulation is quite different from the two-tone behavior, thus illustrating our initial idea and mathematical analyses. These indicate that a calibration for the one-tone case will not guarantee the correct calibration for more complex forms of excitations.



(a)



(b)

Fig. 9 – Simulated results showing the DC voltage measured at the output of the diode power detector with (a) one- and (b) two-tone excitation. The various shades on the graph are included to aid in discerning similar DC output levels of the probe. The absolute scale corresponding to the colors is not significant.

IV. SIMULATION OF PROBE BEHAVIOR IN PRESENCE OF SIGNALS WITH DIFFERENT STATISTICAL CHARACTERISTICS

Until now we have evaluated the behavior of diode probes with changes in the bandwidth of the excitation signal. Nevertheless, modern wireless signals are also imposing strong amplitude variations over time. The effects of these signals on system behavior can be evaluated by studying its statistical pattern. One-tone calibration procedures, due to their constant amplitude, may significantly reduce the accuracy of the calibration.

Thus, the analysis of the behavior of power probes when excited with different PAPR values should also be studied, and carefully evaluated when compared with a one-tone excitation.

Continuing further with the study of the nonlinear terms that will fall on DC, again using expressions (4)-(7), we see that for a two-tone signal, we will have the impact of the difference frequency. As discussed before, the phase of each contribution is always equal, that is the mixing products do not depend on the relative phase between tones. Both $H_2(\cdot)$ and $H_4(\cdot)$ will multiply by $A_1A_1^* = |A_1|^2$, or $A_2A_2^* = |A_2|^2$ in the second-order terms and by $A_1A_1^*A_2A_2^* = |A_1|^2|A_2|^2$ in the fourth-order term, which means that they are independent of the phase of either.

However, if a more complex and rich signal is inserted in the system, such as, for instance, a uniform multisine [11], the outcome will be somewhat different. In order to explain this phenomenon, consider Fig. 10.

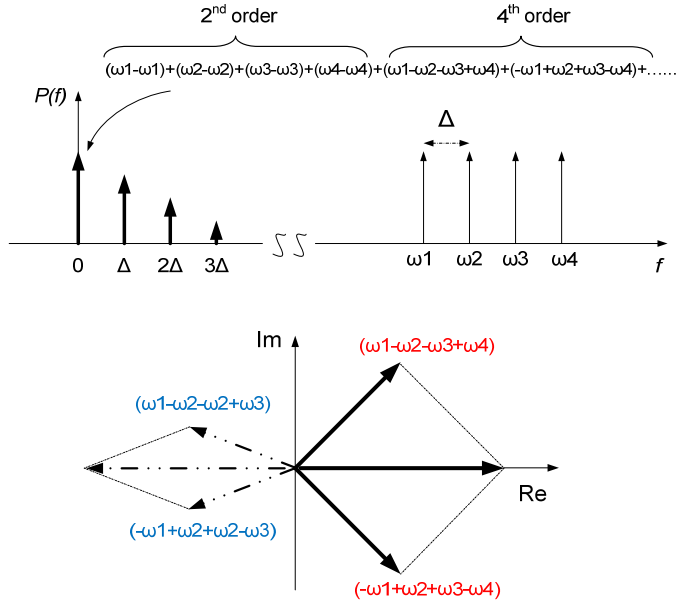


Fig. 10 – Example of second- and fourth-order products at DC with a four-multisine excitation signal.

As seen in Fig.10, the DC component will depend on several terms that are, in turn, dependent on the phase relationship between tones in the multisine. This can result in values of the DC voltage that are not the true average RF power.

For instance, as shown in Fig.10, a fourth-order product resulting from the combination of $\omega_1-\omega_2-\omega_3+\omega_4$ could have a phase that actually is different from 0° . This is counter-intuitive, because we will apparently have a DC component that has a phase different from 0° or 180° : a complex number! To explain this, we note that because the signal is real, a similar component arising from $-(\omega_1-\omega_2-\omega_3+\omega_4)$ is exactly equal to the previous component at this frequency, but complex conjugated. Their addition will become a real number, as expected.

However, the amplitude will be substantially different depending on the phases arising from each tone as seen in Fig.10. Eventually, the resulting vector may even be negative and affect the DC voltage that is measured at output diode probe.

To take this hypothesis further, let us generate several different multisines, using different phase arrangements between tones, but with equal amplitudes. If this signal is measured using a spectrum analyzer the power spectral density will be equal for all the different multisines.

The three generated multisines are: a constant-phase multisine, where a 0° relative phase exists between tones presenting a PAPR of 10 dB; a normal (Gaussian) distribution of relative phases with a PAPR of 5.6 dB, and a uniform distribution of relative phases presenting a PAPR of 3.3 dB. Their statistical probability density functions are present in Fig. 11.

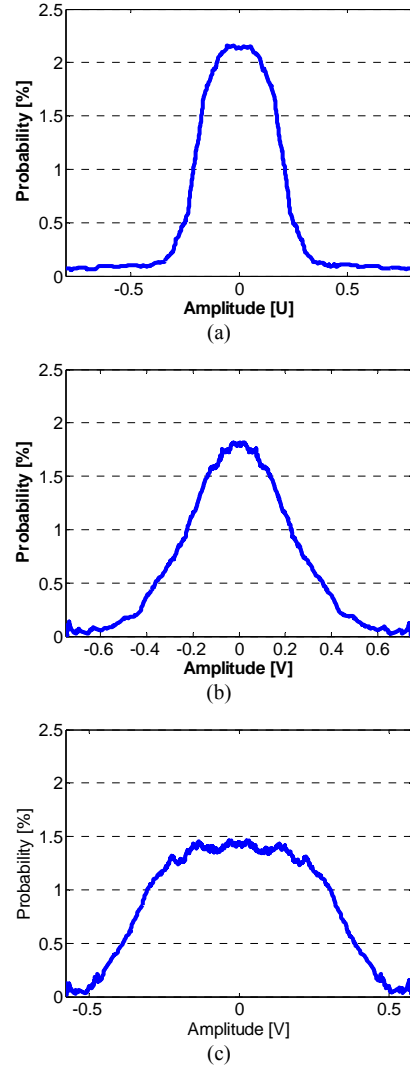


Fig. 11 – Probability density functions of the relative phase distributions of three multisine signals: a) 0° constant; b) normal; c) uniform.

In Fig. 12 the simulated DC values for a 10 component multisine signal having a normal phase distribution is presented. We again see the effect of the load’s low-frequency resonances as was seen in the two-tone case. This indicates that memory effects are appearing also in multisine scenarios.

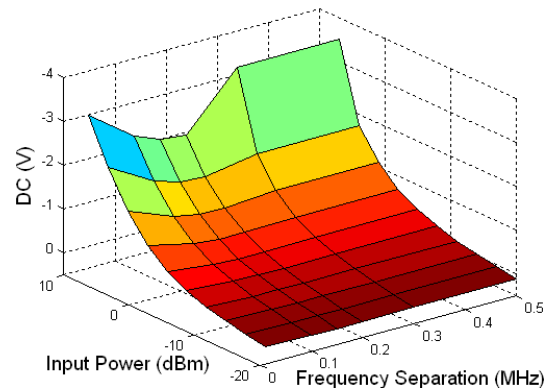


Fig. 12 – Simulation results for a multisine signal excitation with normal phase distribution.

The three multisines were simulated for a small frequency separation, where the resonance will have a mild impact in the final results. Fig. 13 presents the simulated results, and, as discussed previously, the measured DC value is different for each phase distribution.

From Fig. 13, it is also clear that for low values of input power, where the second-order term is dominant, the DC voltage is similar for all of the phase arrangements. The measured voltage only starts to deviate for high values of input power, where higher-order terms start to be important, as was previously explained.

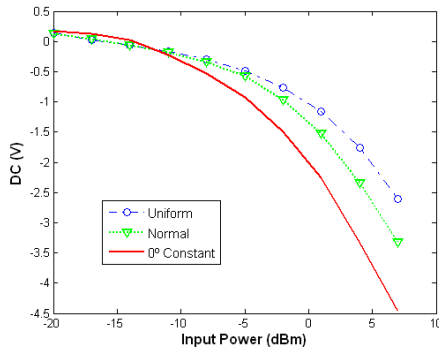


Fig. 13 – Simulation results with the three different multisines for 10 kHz separation of the 10 frequency components.

These simulations illustrate the previous assumption and further expand our first thought that a one-tone excitation is not sufficient for a diode power probe calibration when it is to be used with modulated signals.

V. MEASUREMENTS OF THE BANDWIDTH EFFECT

The circuit of Fig. 4 was fabricated and tested under the same conditions used in the simulations described above. The circuit is presented in Fig. 14. Our measurement set-up (Fig. 15) consisted of two RF sources to generate a two-tone signal, a spectrum analyzer, and a voltmeter. The results presented here are intended to illustrate the trends regarding the use of different excitation signals on measurements made with diode power probes. The goal of the present work is to illustrate qualitative trends on the effects of excitation characteristics on diode power probe measurements. The measurements are not calibrated and measurement uncertainties are not reported. Calibration of such measurements will be the subject of future work.

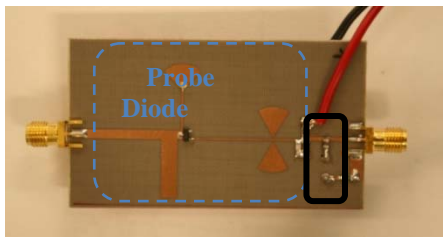


Fig. 14 – Power probe prototype used in laboratory tests.

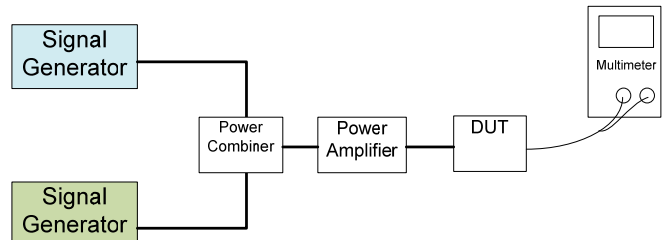


Fig. 15 - Block diagram of the laboratory measurement set-up for the two-tone measurement. In the case of multisines, only one signal generator was used, based on an arbitrary waveform generator.

First the output impedance of the diode power detector was measured with a vector network analyzer. This measurement was made both with and without a multimeter attached. Because the measurements were made at baseband frequencies, the multimeter’s output impedance can actually play an important role, as shown in Fig. 16.

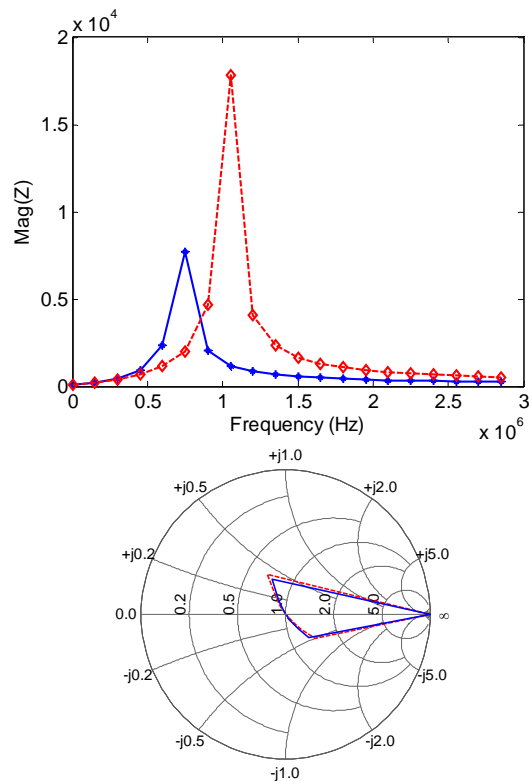
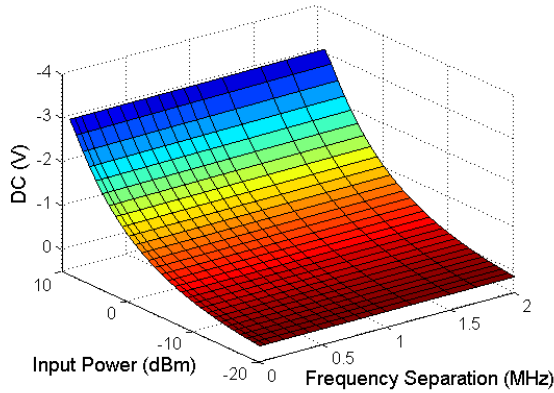


Fig. 16 – VNA measurements of the diode power detector’s output load impedance: without multimeter attached (red dashed) and with multimeter attached (blue solid).

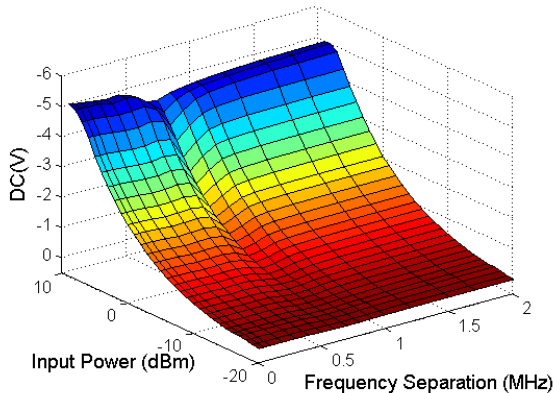
In Fig. 17 (a) and 17 (b), the measurement results for a single sinusoidal signal and two-tone excitation are presented, respectively. The measured results are based on the assumptions that the DC voltmeter and signal generator are operating within manufacturers’ specifications ($\pm 0.7\%$ for the DC voltmeter, and <0.9 dB for the signal sources), and that the sources of random error are negligible.

As can be seen in these figures, we observe a change in the DC value of almost 1 volt near the resonance frequency. The resonant frequency values are not equal to the simulated ones because of an inexact representation of the baseband impedance in the simulations. However, these results

demonstrate our initial assumption, that if the probe is calibrated with a single tone, it can give incorrect results when excited by a two-tone signal when the baseband impedance is a function of frequency, as is often the case for reactive matching networks.



(a)

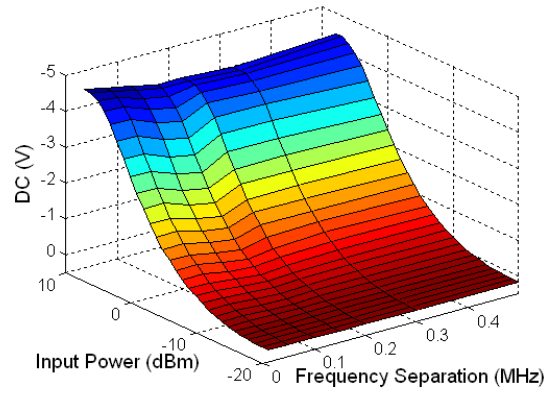


(b)

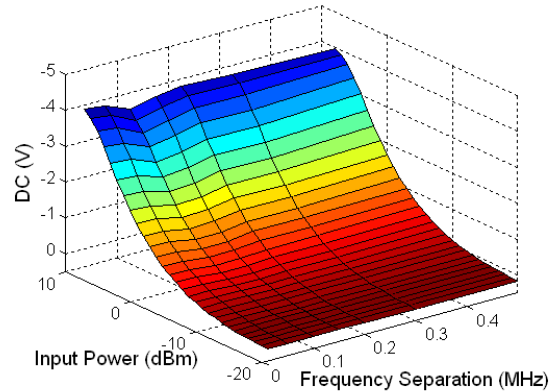
Fig. 17 – Illustrative measurement results with one-tone (a) and two-tone (b) excitations.

VI. MULTISINE MEASUREMENTS

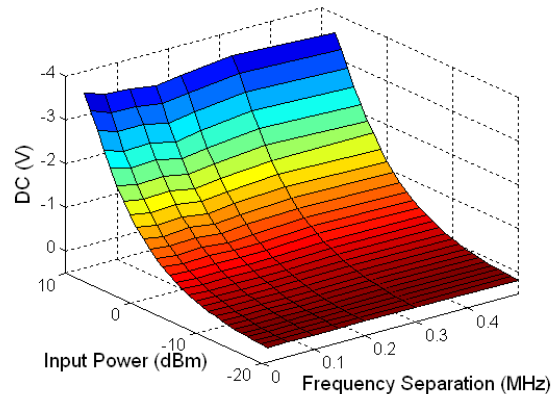
We now analyze the response of our probe to the multisine signals described in Section IV to study the effect of different PAPR values. We also varied the multisines in both tone separation and power. Figs. 18-19 present the results for the three multisines.



(a)



(b)



(c)

Fig. 18 – Illustrative measurement results using multisine excitations with: (a) constant phase (0°); (b) normal phase distribution (c) uniform phase distribution.

From the figures, a similar behavior can be seen as in the two-tone cases, that is the graphs present a dip at a tone spacing on the order of the resonant frequency value. We also see that in the multisine case the dip is wider. This can be attributed to the fact that even if the tone separation is smaller than the resonant frequency, the signal can also present several multiples of the tone separation, some of which will fall on the resonant frequency. This effect will not occur for a two-tone excitation signal, because only one tone separation appears.

Even though we always excited the circuit with a ten-tone multisine having the same amplitude for each tone, the output DC values were different for each statistical arrangement. As a result a different power value will be reported for each multisine, even though the power should be equal for all of the excitations.

In order to better understand the effects of the statistical distribution in the nonlinear behavior of the different multisines, a plot of the DC power for each multisine is presented in Fig. 19.

As can be seen, for low values of power, each distribution provides similar results. But when the signal power increases the nonlinear behavior of the probe is excited. In this case, the obtained results present different behaviors. The DC values are also different in Fig. 19 (a) and (b), corresponding to a different frequency separation, as expected.

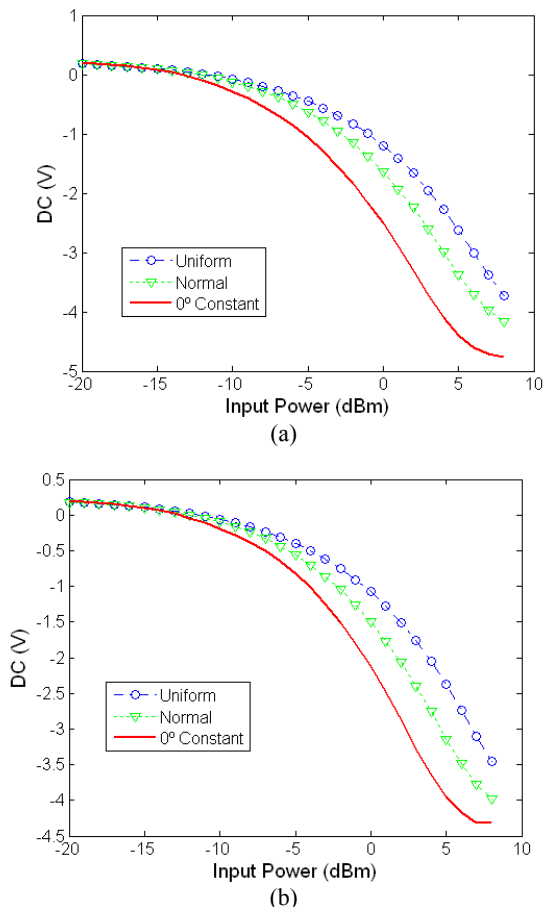


Fig. 19 – Qualitative comparison of measurements made with the power probe of multisines having three relative phase distributions: (a) for 10kHz separation between the tones; (b) for a separation between the tones corresponding to the resonant frequency.

VII. PROBE BEHAVIOR UNDER WIRELESS SIGNAL EXCITATION

Finally, and in order to evaluate the previous developed analysis with real signals, two digitally modulated signals were used, quadrature-phase-shift-keyed (QPSK) with around 4 dB PAPR and 256-quadrature-amplitude-modulation (QAM) modulation types with around 12 dB PAPR. These

modulations were selected due to their difference in PAPR values.

Both of the signals were generated using a vector signal generator over different bandwidths and with the same integrated average power. Fig. 20 presents the measured results.

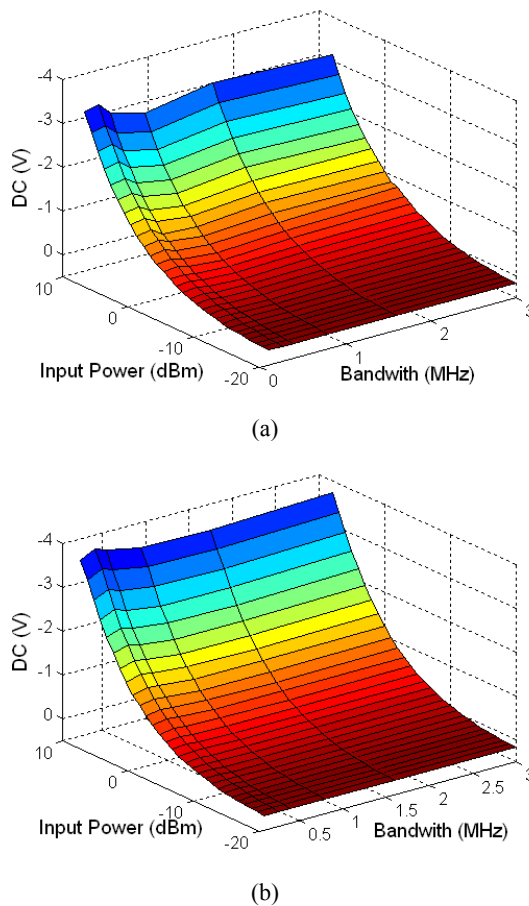


Fig. 20 – Illustrative power-probe measurement results using (a) QPSK signal; (b) 256-QAM signal.

As can be seen from Fig. 20, similar results are obtained as those predicted from the previous analyses, in this case a dip continues to be visible when the bandwidth of the signals is changed. The DC value is also different for the different modulation formats. This can also be seen in Fig. 21, which illustrates once again that the probe is sensitive to both PAPR and signal bandwidth.

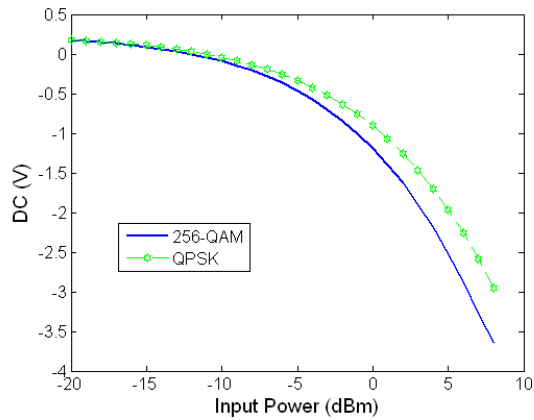


Fig. 21 – Qualitative comparison of power probe measurements of the two digitally modulated signals as a function of input power.

VIII. CONCLUSION

This paper analyzed issues on the use of diode power probes for measuring signals corresponding to new wireless standards. Two different aspects were studied, the effect of the signal's bandwidth and its PAPR on the power measurement.

Our analyses demonstrated mathematically, by simulations and by measurements, that the calibration of a power probe with a single-tone excitation does not guarantee the correct calibration for more complex forms of excitations. This was then illustrated through measurement with digitally modulated signals, including a QPSK signal and a 256-QAM signal.

This paper also leads to the conclusion that a proper design of the diode power probe in order to account for low values of baseband impedance covering all the signal bandwidth is necessary. As well, the different values obtained with signals presenting high values of PAPR should be compensated for with different calibration approaches. Such calibrations and measurement uncertainties are the subject of current research and will be presented in future work.

ACKNOWLEDGMENTS

This work was partially supported by projects TEC2008-06874-C03-02-FEDER, INCITE08PXIB322241PR, Acción Integrada (HP2006-120) and TACCS – PTDC/EEA-TEL/099646/2008. Partial work of the U.S. government, not subject to copyright in the United States

REFERENCES

- [1] M. Kanda and L.D. Driver, "An isotropic electric-field probe with tapered resistive dipoles for broad-band use, 100 kHz to 18 GHz", *IEEE Trans. Microwave Theory Tech.*, vol. 35, no. 2, pp 124- 130, Feb 1987.
- [2] M. Kanda, "Standard probes for electromagnetic field measurements", *IEEE Trans. Antennas Prop.*, vol. 41, no. 10, pp. 1349-1364, Oct 1993.
- [3] J.M. Ladbury and D.G. Camell, "Electrically short dipoles with a nonlinear load, a revisited analysis," *IEEE Trans. Electromagnetic Compatibility*, vol. 44, no. 1, pp. 38-44, Feb 2002.
- [4] J. C. Pedro and N. B. Carvalho, *Intermodulation Distortion in Microwave and Wireless Circuits*, 1st ed. Norwood, MA: Artech House, 2003.
- [5] C. D. Nallo and A. Faraone, "Effect of amplitude modulation of the CDMA IS-95 signal on SAR measurements," *IEEE Trans. Electromagnetic Compatibility*, vol. 48, no. 3, pp. 552-562, Aug. 2006.
- [6] N. B. Carvalho and J. C. Pedro, "A comprehensive explanation of distortion side band asymmetries," *IEEE Trans. Microwave Theory Tech.*, vol. 50, no.9, pp. 2090-2101, Sept. 2002.
- [7] S. H. Han and J. H. Lee, "An overview of peak-to-average power ratio reduction techniques for multicarrier transmission," *IEEE Trans. Wireless Comm.*, vol. 12, no. 2, pp. 56 – 65, April 2005.
- [8] H. Gomes, A. R. Testera, N. B. Carvalho, M. F. Barciela and K. A. Remley, "The impact of long-term memory effects on diode power probes", *IEEE Int. Microwave Symp. Dig*, May, 2010, Anaheim, CA, USA.
- [9] D. Adamson, D. Bowns, A. Fernández, E. Goodall, D. Humphreys, "The response of electric field probes to realistic RF environments," *IEEE Int. Microwave Symp. Dig*, May, 2010, Anaheim, CA, USA.
- [10] A. Rodriguez-Testera, O. Mojon, M. Fernandez-Barciela, E. Sanchez, "Robust packaged diode modelling with a table-based approach", *Proc. European Microwave Integrated Circuit Conf., EuMIC*, 27-28 Oct. 2008, pp. 131-134, Amsterdam, Netherlands.
- [11] N.B. Carvalho, K.A. Remley, D. Schreurs, and K.C. Gard, "Multisine signals for wireless system test and design," *IEEE Microwave Mag.*, vol. 9, no. 3 pp. 122 – 138, June 2008.